Biosensors and Bioelectronics 143 (2019) 111610

Contents lists available at ScienceDirect

Biosensors and Bioelectronics

journal homepage: www.elsevier.com/locate/bios

Label-free and ultrasensitive electrochemical biosensor for the detection of EBV-related DNA based on AgDNCs@DNA/AgNCs nanocomposites and lambda exonuclease-assisted target recycling

Haiying Que[a,1], Decai Zhang[a,b,1], Bin Guo[a], Tong Wang[a], Haiping Wu[a], Daobin Han[a], Yurong Yan[a,*]

[a] Key Laboratory of Clinical Laboratory Diagnostics (Ministry of Education), College of Laboratory Medicine, Chongqing Medical University, Chongqing, 400016, China
[b] Department of Laboratory Diagnosis, The Third Affiliated Hospital of Shenzhen University, Shenzhen University, Shenzhen, 518000, China

ARTICLE INFO

Keywords:
Electrochemical biosensor
pDNA-AgDNCs@DNA/AgNCs conjugates
Lambda exonuclease
Epstein-Barr virus
DNA detection

ABSTRACT

A label-free and efficient electrochemical biosensor was developed for the ultrasensitive detection of EBV-related DNA by combing AgDNCs@DNA/AgNCs nanocomposites with noncanonical lambda exonuclease (λ exo)-assisted target recycling (LNTR). The conjugates of AgDNCs, DNA/AgNCs and probe DNA (pDNA-AgDNCs@DNA/AgNCs conjugates) worked as not only ideal nanocarriers but also efficient electrochemical tags. LNTR didn't require phosphorylated substrates and could be triggered specifically by target DNA, leading to the recycling use of target DNA and the liberation of plentiful linker probes (LP). Subsequently, the LP hybridized with the capture probes on the electrode and then bond to pDNA-AgDNCs@DNA/AgNCs conjugates, generating a sensitive electric signal directly. What's more, the signal amplification effects of DNA/AgNCs and LNTR were investigated. Under the optimal conditions, the proposed method exhibited a wide linear range of 1 fM to 1 nM and the detection limit down to 0.38 fM. In addition, the developed biosensing method exhibited excellent specificity and was successfully applied to detect target DNA in complex biological matrix. The proposed biosensor without extra bio-labels may provide a promising platform in bioanalysis and biochemical research.

1. Introduction

With the development of nanomaterials science, a diversity of nanomaterials, such as DNA self-assembly nanostructures, metal nanocomposites and polymers, have been widely utilized in the field of sensing analysis and cancer therapy (Bian et al., 2019; Tang et al., 2018; Zhou et al., 2016). Among them, silver nanomaterials are a kind of most commonly used materials owing to their high extinction coefficient, controllable particle size and facile synthesis (Liu and Huang, 2012; Miao et al., 2018). Nowadays, silver nanomaterials are of considerable interest as electrochemical tags for developing label-free electrochemical biosensors. For instance, Kangkamano et al. adopted silver nanofoam as stationary redox indicator to develop a label-free electrochemical biosensor for microRNA detection (Kangkamano et al., 2018). Favorably, silver-based electroactive tags have the inherent advantages of good biocompatibility, high conductivity and amplified electrochemical signal (Maduraiveeran et al., 2018). But the lack of stability and easy oxidation still restrict their application in biosensing technology.

Various templates have been employed to protect silver nanocomposites from aggregation and oxidation, including polyelectrolyte, dendrimers, thiol-compounds, DNA and lysozyme (Lyu et al., 2019; New et al., 2016; Zhou et al., 2012b). As a soft template, DNA has structural diversity and ease of integration with aptamers for biorecognition. DNA-encapsulated Ag nanoclusters (DNA/AgNCs) with 2 nm in diameter are composed of several silver atoms, possessing good electronic properties and bright fluorescence properties (Hu et al., 2017; New et al., 2016). Although DNA/AgNCs are more prone to the fluorescence detection, several reports showed that DNA/AgNCs can be effective electrochemical probes and remarkable electrocatalysts in the fabrication of electrochemical biosensor (Chen et al., 2015, 2018). However, most of DNA/AgNCs-based electrochemical methods require more than 4 h to grow super-sandwich DNA structure and prepare DNA/AgNCs on the electrode surface, which are time-consuming and fussy (Jie et al., 2017; Peng et al., 2018; Yang et al., 2015). And the sensitivity of the biosensor based on single template stabilized silver

* Corresponding author.
E-mail addresses: yanyurong@cqmu.edu.cn, yanyurong163@163.com (Y. Yan).
[1] These authors contributed equally to this work.

https://doi.org/10.1016/j.bios.2019.111610
Received 24 June 2019; Received in revised form 7 August 2019; Accepted 17 August 2019
Available online 19 August 2019
0956-5663/

nanoprobe is rather limited (Dong et al., 2012). To some extent, the dual template-encapsulated silver nanocomposites may be highly efficient signal indicators for timely and direct signal transduction. As novel three-dimensional polymers, polyamidoamine (PAMAM) dendrimers hold several remarkable features of monodispersion, chemical stability and good biocompatibility (Huang et al., 2005; Sorsak et al., 2015). Metal/dendrimers nanocomposites possess the advantages of long-term stability and the possibility of multiplex assay by loading dendrimers with various host metals (Stofik et al., 2009). Hundreds of hydrophilic terminal functional amino-groups make PAMAM dendrimers excellent carriers for immobilizing probe DNA (pDNA) and DNA/AgNCs. Therefore, with the increased loading surface for silver, the conjugates of PAMAM dendrimers-encapsulated silver nanocomposites (AgDNCs) linked with DNA/AgNCs and pDNA (pDNA-AgDNCs@DNA/AgNCs conjugates) can be greatly enhanced electrochemical tags. More importantly, the developed tags able to generate DPV signal directly without the addition of external signaling species.

Sandwich electrochemical biosensor, endowed with low background, small dimension and simple design, is a powerful technology for nucleic acid analysis (Aoki, 2015). Unfortunately, the biosensing sensitivity are strongly limited because each target molecular can only bind to single capture probe and signal probe (Zhou et al., 2012a). Numerous researches have been carried out to improve the sensitivity of the sandwich method, including λ exo-aided target recycling, entropy-driven amplification reaction as well as cascade signal amplification of strand displacement polymerization and rolling circle amplification (RCA) (Li et al., 2016; Shi et al., 2018; Zhang et al., 2019). Although the reported methods are featured by high sensitivity, good adaptability and efficiency, some special requirements such as the ligation of a padlock probe, specially modified substrates and rigorous sequence design increase the complexity and cost of the experiment. Thus, developing a sensitive isothermal amplification method with facile design and no modification is important to simplify detection process. Generally, λ exo prefers double-strand DNA (dsDNA) with one 5′-PO_4 and proceeds to hydrolyze 5′-PO_4 DNA strand in the direction of 5'→3′ end (Kovall and Matthews, 1997). Therefore, commonly used λ exo-aided target recycling highly depends on 5′-PO_4 substrates (Liu et al., 2016; Shi et al., 2018). Interestingly, the lately report disclosed a noncanonical property of λ exo, which a dsDNA with a two-nucleotide (2 nt)-protruding end can be digested by λ exo with high efficiency (Wu et al., 2018).

Herein, pDNA-AgDNCs@DNA/AgNCs conjugates and noncanonical lambda exonuclease (λ exo)-assisted target recycling (denoted as LNTR) have been firstly employed to fabricate a label-free and ultrasensitive electrochemical nucleic acid biosensor. Epstein-Barr virus (EBV)-related DNA was used as a model analyte, which associated with several malignancies as Hodgkin's disease, Burkitt's lymphoma and nasopharyngeal carcinoma (Balvedi et al., 2014). The strategy achieves ultrasensitive detection of EBV-related DNA with excellent specificity, which holds a great potential for early diagnosis of EBV-related diseases.

2. Experiment section

2.1. Materials and reagents

λ exo and 10 × λ exo reaction buffer (670 mM glycine-KOH, 25 mM $MgCl_2$, 500 μg mL^{-1} BSA, pH 9.4) was purchased from New England Biolabs (Beverly, MA, USA). 6-Mercapto-1-hexanol (MCH), amine-terminated G5.0 PAMAM ethylenediamine core type and tris (2-carboxyethy) phosphine hydrochloride (TCEP) were purchased from Sigma-Aldrich (St. Louis, USA). 1-ethyl-3-[3-dimethylaminopropyl] carbodiimide hydrochloride (EDC) was purchased from Sangon Inc. (Shanghai, China). Silver nitrate ($AgNO_3$) was purchased from Guanghua Technology Co., Ltd. (Guangdong, China). Sodium borohydride ($NaBH_4$) was purchased from Kelong Chemical Company (Chengdu, China). Both ethanol precipitation kit and DNA Ladder Marker (20 bp) were purchased from TaKaRa (Dalian, China). GoldView I was purchased from Solarbio Technology Co., Ltd. (Beijing, China). All synthesized DNA oligonucleotides purified by high-performance liquid chromatography (HPLC) (listed in Table S1) were obtained from Sangon Inc. (Shanghai, China).

Washing buffer (pH 7.4) contained 20 mM Tris, 0.1 M NaCl, 5 mM $MgCl_2$ and 0.05% Tween-20.1 × TE buffer (pH 8.0) contained 10 mM Tris HCl and 1 mM EDTA. 0.1 M phosphate buffer (PB) (pH 7.0) comprised 0.01 M Na_3PO_4 and 0.1 M NaCl. 0.3 M PB (pH 7.0) contained 0.01 M Na_3PO_4 and 0.3 M NaCl. All other reagents were of analytical grade and Milli-Q water (≥18.2 MΩ cm^{-1}) were used for all solutions.

2.2. Instruments

All electrochemical analyses were carried out on a CHI660D electrochemical workstation (Shanghai Chenhua Instruments Co. Ltd., China) with gold working electrode (3 mm in diameter), saturated calomel reference electrode and platinum wire auxiliary electrode. Measurements of fluorescence spectra and UV–vis absorption spectra were recorded by a Cary Eclipse Fluorescence Spectrophotometer (Agilent Technologies, Palo Alto, CA) and UV-2250 spectrophotometer (Shimadzu, Japan), respectively. The surface morphologies and lattice images were measured on a field emission electron microscope JEM 2100 (JEOL, Ltd., Japan) operated with 200 KV accelerating voltage. DNA suspensions were quantified by a NanoDrop 1000 spectrophotometer (Thermo Scientific, USA). The gel electrophoresis analysis was operated on an electrophoresis analyzer (Bio-Rad, USA). Gel image was obtained from an imaging system (Bio-Rad Laboratories, USA).

2.3. Synthesis of AgDNCs

AgDNCs were synthesized according to previous reports with the slight modification (Jin et al., 2018). Briefly, 66.7 μL of dendrimers (1.5 mM) were mixed with 300 μL $AgNO_3$ solution (10 mM) to form Ag^+/dendrimers complex under continuously stirring for 20 min. Subsequently, 120 μL newly prepared $NaBH_4$ solution (50 mM) was added dropwise into Ag^+/dendrimers mixture with continuously stirring for 40 min to reduce Ag^+ *in situ*. Afterwards, the resulted solution changed to brown yellow, indicating the reduction of Ag^+ to Ag^0 and the formation of AgDNCs. All steps were carried out at room temperature. The prepared AgDNCs solution can be stored at 4 °C in the dark for at least two weeks without color change and precipitation.

2.4. Synthesis of DNA/AgNCs

DNA/AgNCs were synthesized according to the reported method (Lee et al., 2017; Miao et al., 2018). The molar ratio of DNA template/$AgNO_3$/$NaBH_4$ was 1:6:6, finally. In general, 40 μL of $AgNO_3$ solution (300 μM) was initially added into 40 μL of DNA template (Table S1) solution (50 μM) and vortexed vigorously for 30 s, then incubated at 4 °C in the dark for 15 min to form DNA-Ag^+ complex. Subsequently, 40 μL of newly prepared $NaBH_4$ solution (300 μM) was quickly added to the mixture to reduce Ag^+. After vortexed vigorously for 30 s, the resulting solution was stored at 4 °C in the dark for at least 4 h to generate stable DNA/AgNCs.

2.5. Preparation of pDNA-AgDNCs@DNA/AgNCs conjugates

The G5.0 amine-terminated PAMAM dendrimers have hundreds of hydrophilic terminal functional amino-groups on its exterior (Qiu et al., 2016). The pDNA-COOH and DNA/AgNCs–COOH were modified to the as-prepared AgDNCs simultaneously *via* amidation reaction among AgDNCs, pDNA and DNA/AgNCs. Conjugation of pDNA, DNA/AgNCs and AgDNCs was performed by adding 100 μL 133 nM linker probes (LP) and 100 μL 67 nM DNA/AgNCs to 2 mL solution of AgDNCs containing 1 mM EDC for about 10 h with gentle stirring at ambient

temperature. After centrifuged at 16,000 g for 20 min, the supernatant was discarded, resulting the resuspended conjugates by adding 400 μL 0.3 M PB (pH 7.0). The prepared pDNA-AgDNCs@DNA/AgNCs conjugates solution was stored at 4 °C until further use.

2.6. Noncanonical lambda exonuclease (λ exo)-assisted target recycling (LNTR)

Prior to use, the mixture of the protruding probes (PP) and LP solution at 1:1 M ratio was heated at 95 °C for 5 min, followed by chilling it to room temperature slowly to form a stable duplex strand complex (DSC). The analytical procedure of LNTR was detailed as follows: the mixture of DSC (0.5 μM), λ exo (0.20 unit μL^{-1}) and 20 μL various concentration of the EBV-related DNA in 1 × λ exo reaction buffer was premixed (the total volume was 50 μL). Then, the mixture was incubated at 37 °C for 100 min to liberate massive LP. After that, the mixture was heated to 85 °C for 5 min to deactivate λ exo. In order to reduce the unstable effects of the enzymatic buffer on the electrode, the products of LNTR were purified by ethanol precipitation kit (shown in supporting information) and dissolved in 50 μL of 1 × TE buffer (pH 8.0).

2.7. Fabrication of the electrochemical DNA biosensor and electrochemical analyses

At first, gold electrodes (GE, 3 mm in diameter) were polished with 0.05 μm alumina powder for 5 min to a mirror, followed by sonication in ultrapure water, absolute ethanol and ultrapure water for 5 min, respectively. GE were then soaked in piranha solution for 10 min and rinsed thoroughly with ultrapure water for eliminating other impurity. 0.5 μM capture probes (CP) were pretreated by TECP (50 μM) for 1 h in room temperature to break disulfide bond. Subsequently, 10 μL of 0.5 μM CP were dropped on the cleaned electrode followed by the incubation at 4 °C overnight. The electrodes were rinsed with washing buffer and then covered with 10 μL of 1 mM MCH to block the unbinding sites. After being rinsed with washing buffer, the MCH/CP modified electrodes were incubated with 10 μL of the purified reaction products of LNTR for 40 min at 37 °C in order to capture LP. Finally, followed by washing with washing buffer, the electrodes were incubated with 10 μL of fixed concentration of pDNA-AgDNCs@DNA/AgNCs conjugates at 37 °C for 1 h. The resulted electrodes were washed with 0.1 M PB (pH 7.0) and electrochemical measurements were performed. The differential pulse voltammetry (DPV) signal could be easily recorded in 0.1 M PB (pH 7.0) by scanning it from −0.2 V to 0.3 V, with amplitude 50 mV, pulse width 16.7 ms and pulse period 200 ms.

2.8. Native polyacrylamide gel electrophoresis

The 12% native polyacrylamide gel was prepared to verify the hydrolysis behavior of λ exo toward DSC with 2-nt overhang in the presence of target DNA. Electrophoresis was carried in 1 × TBE buffer (2 mM EDTA, 89 mM Tris-boric acid, pH 8.3) at a 100 V constant voltage for 45 min. Then, the gel was immersed in a freshly prepared stain-all solution (80 mL of 1 × TBE buffer containing 4 μL of GoldView I) for 30 min. Afterwards, the gel was imaged using gel image system.

3. Results and discussion

3.1. The configuration of sandwich electrochemical DNA biosensor

As depicted in Scheme 1A, AgDNCs and DNA/AgNCs were synthesized from PAMAM dendrimers and cytosine-rich DNA through *in situ* reduction. pDNA-AgDNCs@DNA/AgNCs conjugates were obtained by covalently cross-liking pDNA and DNA/AgNCs to the surface of PAMAM dendrimer. The AgDNCs could directly serve as electrochemical tags for signal output. Meanwhile, PAMAM dendrimers in AgDNCs were utilized as nanocarriers for immobilizing the excellent electroactive DNA/AgNCs and the recognition probes of pDNA, loading more silver nanoclusters for signal amplification. The overall principle and sandwich biosensing step were shown in Scheme 1B, initially, the thiolated CP were immobilized on a cleaned gold electrode via Au–S bond and then blocked the unbinding sites with MCH. Hereafter, in LNTR thermal system, PP as hydrolyzed substrate of λ exo, including two mismatched bases at 5′ end (in red), a target DNA recognition domain (in yellow green) and LP binding domain (in black). LP has two domains (in purple and green) to bind with CP and pDNA, respectively. Before recycling, LP hybridized with PP to form DSC as an initial machine. The LNTR owns the merits of target recycling, simple and flexible, no modification, no ligation of a padlock probe and no need for polymeric substances. In the presence of target DNA, λ exo attracted to the 2-nt overhang of PP and digested PP stepwise in the direction of 5'→3' end, liberating LP and recycling use target DNA. Followed, the released LP hybridized with CP and then bind to pDNA-AgDNCs@DNA/AgNCs conjugates. Benefiting from dual-template enhanced electrooxidation effects and target recycling, a small quality of target DNA could be transformed into a mass silver-based electric signal. The method achieved the quantification of EBV-related DNA down to 0.38 fM without super-sandwich structure assisted amplification and phosphorylated substrates. Thus, this biosensor provides a label-free, isothermal and facile method for ultrasensitive detection of EBV-related DNA.

3.2. Characterization of nanomaterials

UV–vis absorbance spectrum was used to characterize the successful synthesis of DNA/AgNCs (Fig. 1A). Peak a at 260 nm represented typically the absorption of DNA template (Mu et al., 2018). Peak c at 540 nm indicated the formation of ultra-small Ag nanoclusters using DNA template and similar to their excitation spectra (Fig. 1B, curve a). While peak b represented the large Ag nanoparticles resulted by the aggregation of silver atoms (Han and Wei, 2018). DNA/AgNCs were transparent under daylight and exhibited a bright red color under UV light. What's more, the fluorescent spectrum of DNA/AgNCs showed that DNA/AgNCs had maximum emission at 620 nm (Fig. 1B, curve b) when excited at 540 nm (Fig. 1B, curve a), which were consistent with the reported literature (Lee et al., 2017). We also performed the UV–vis absorbance spectrum to investigate whether the pDNA-AgDNCs@DNA/AgNCs conjugates were successful assembled (Fig. S1).

The formation of DNA/AgNCs was also evidenced by the HRTEM images which clearly showed that the formed Ag nanoclusters were spherical in shape, and average size was about 2 nm (Fig. 2C). The highly paralleled and ordered lattice fringe with the d-spacing of 0.24 nm was observed (Fig. 2C and D), well matching the {110} crystal face of Ag (Zeng et al., 2010). HRTEM images of the synthesized AgDNCs in Fig. 2A indicated uniform and spherical AgDNCs. Fig. 2F showed narrow distribution of 3.81 ± 0.51 nm diameter measured from HRTEM image (Fig. 2A), which was similar to that reported work (Jin et al., 2018). AgDNCs@DNA/AgNCs nanocomposites with good monodispersity were also analyzed by HRTEM and in narrow distribution of 7.19 ± 0.70 nm diameter (Fig. 2E and G).

3.3. Feasibility of EBV-related DNA detection system coupled pDNA-AgDNCs@DNA/AgNCs conjugates and LNTR

Electrochemical impedance spectroscopy (EIS) was first performed to characterize the dynamic assembly process of the electrode surface with 5 mM $[Fe(CN)_6]^{3-/4-}$ in 0.1 M KCl solution. As for EIS, $[Fe(CN)_6]^{3-/4-}$ was a redox probe and the semicircle diameter was expressed as electron transfer resistance (Ret) of the electrode. As depicted in Fig. 3A, the bare GE exhibited a definitely small semicircular domain (curve a) because of the extremely low resistance on the surface of bare GE. After the immobilization of CP on the bare GE, the Ret gave

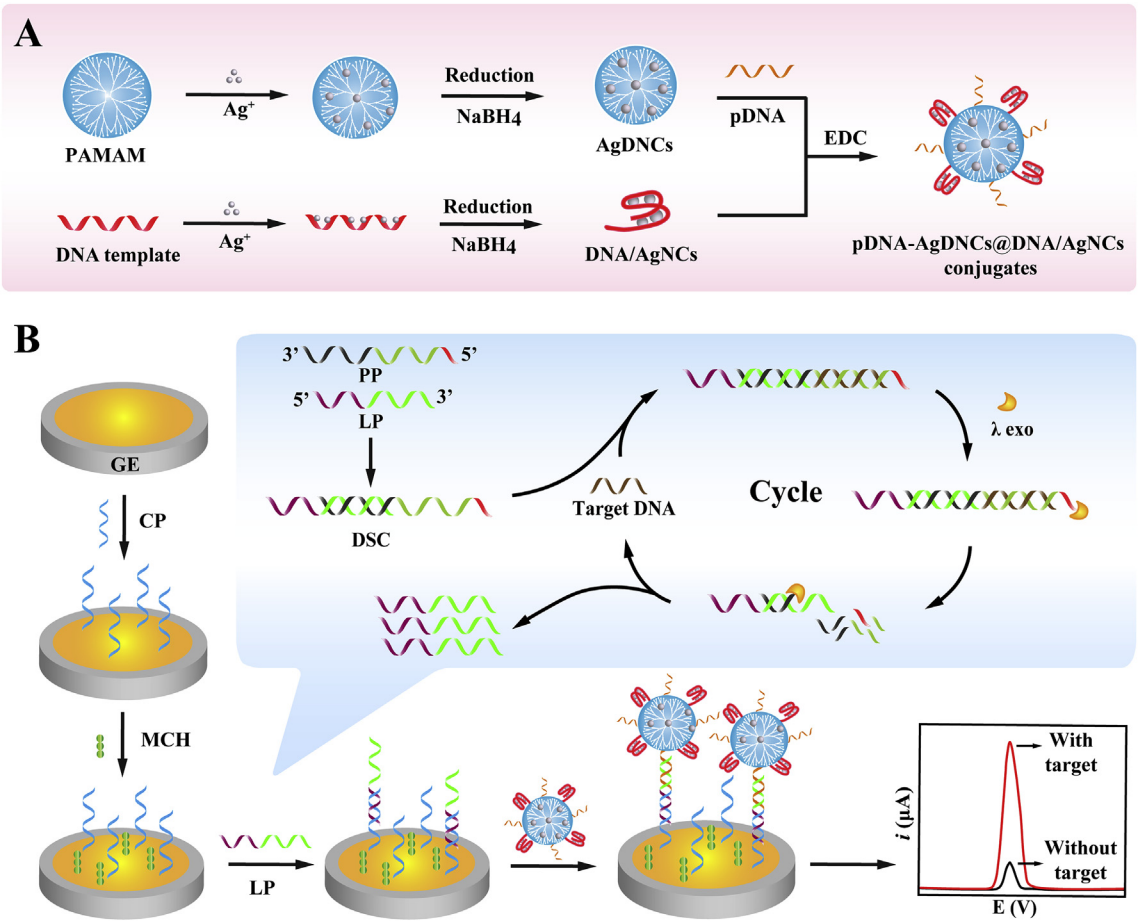

Scheme 1. (A) The preparation of pDNA-AgDNCs@DNA/AgNCs conjugates. (B) Schematic illustration of the biosensing protocol for EBV-related DNA detection based on pDNA-AgDNCs@DNA/AgNCs conjugates and noncanonical λ exo-assisted target recycling.

a rise (curve b) owing to the electrostatic repulsion between $[Fe(CN)_6]^{3-/4-}$ and negatively charged DNA strand. The Ret increased (curve c) after MCH was immobilized on the CP/GE surface because MCH blocked the electron transfer from electrode surface. When the products of LNTR incubated with MCH/CP/GE, the Ret raised obviously (curve d), indicating the successful liberation of LP from LNTR. Afterwards, the Ret decreased dramatically upon the hybridization of pDNA-AgDNCs@DNA/AgNCs conjugates with LP/MCH/CP/GE, which related to the excellent conductivity of silver nanocomposites on PAMAM dendrimers and DNA template. Subsequently, CV was also applied to explore the layer-by-layer assembly process on the electrode surface (Fig. 3B) and in good agreement with the results from EIS. Those results based on EIS and CV proved the successful assembly process of the fabricated biosensor.

Furthermore, the DPV signals under different conditions were performed to demonstrate the signal amplification effect of LNTR and DNA/AgNCs (depicted in Fig. 3C). There was a very small signal appeared in the absence of target DNA (curve a), which related to the inhibition of the LNTR amplification process and the liberation of LP was suppressed. The small background signal may have connections to

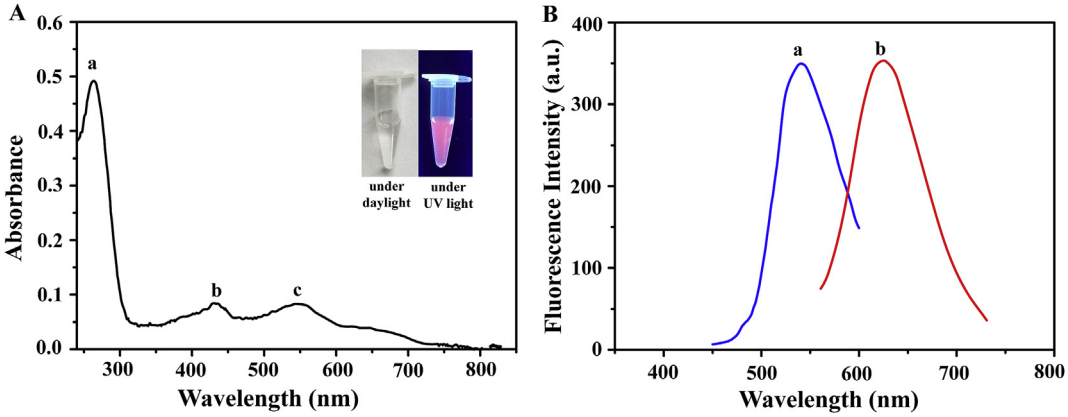

Fig. 1. (A) UV–vis absorption spectrum of DNA/AgNCs. The insert shows photograph of synthesized DNA/AgNCs under daylight (left) and UV light (right). (B) Fluorescence spectra of the fluorescent DNA/AgNCs: curve a and curve b are the excitation and emission fluorescence spectra respectively (λex = 540 nm, λem = 620 nm).

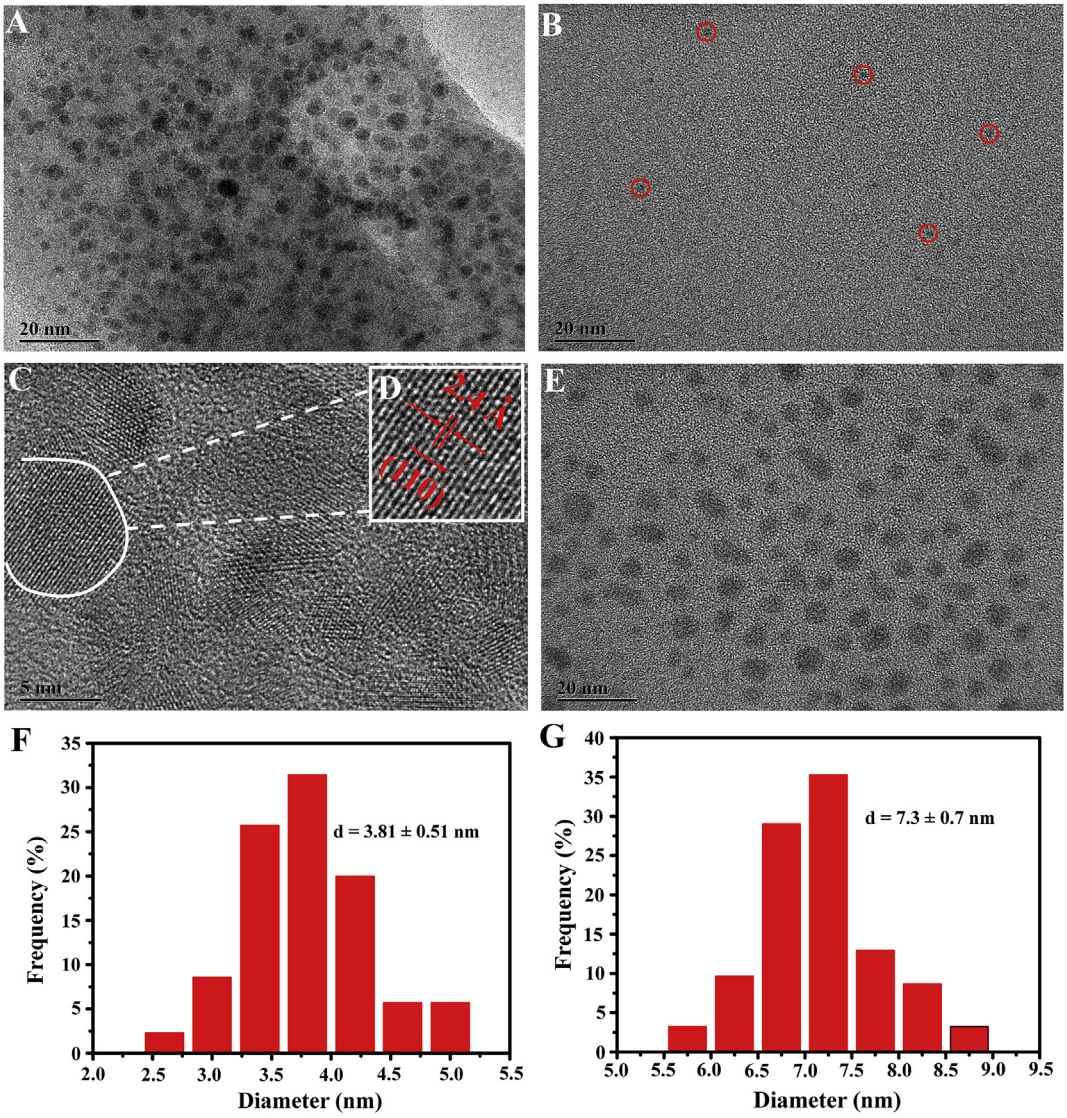

Fig. 2. HRTEM images of (A) AgDNCs, (B) DNA/AgNCs and (E) AgDNCs@DNA/AgNCs nanocomposites in 20 nm scale. (C) HRTEM image of DNA/AgNCs in 5 nm scale and (D) an amplified HRTEM image of DNA/AgNCs. The size distribution histogram of (F) AgDNCs and (G) AgDNCs@DNA/AgNCs nanocomposites.

the electrostatic interaction between Ag^+ (positively charged) which directly adsorbed on the self-assembled MCH/CP/GE and DNA backbones (negatively charged) (Yang et al., 2015). We found that a significantly increased DPV signal was occurred at ~ +0.055 V when the target DNA (1 nM) existed in a complete system (curve d). Another two control experiments without LNTR or DNA/AgNCs were performed. The DPV response of 1 nM target DNA integrated with LNTR (curve d) was about 1.8 times higher than that without LNTR (curve b). The DPV signal without DNA/AgNCs (curve c) was about 1.4 times lower than those with DNA/AgNCs on the overall biosensing system (curve d), ascribing to the electro-oxidation of the DNA/AgNCs in electrochemical biosensing system (Chen et al., 2018). Comparisons indicated the feasibility of λ exo-assisted target recycling and the enhanced electro-oxidation ability of pDNA-AgDNCs@DNA/AgNCs conjugates for developing a dual signal enhancing system.

12% native PAGE was utilized to investigate the LNTR process. As shown in Fig. 3D, the migration speed of stripes in Lane 1 (target DNA), Lane 2 (LP) and Lane 3 (PP) gradually decreased as the increase in the length of the single chain. The hybridization of PP and LP could form a new stripe (DSC) in Lane 4. Only DSC and λ exo existed in the system, the stripe of DSC kept intact, indicating λ exo couldn't hydrolyze PP and LP. This is due to each DNA strand in DSC has the 5′ protruding end that is well beyond 2-nt. When DSC mixed with target DNA in Lane 6, the single stripe of the mixture became stronger than the one in Lane 4. The similar migration speed was related to the same double strand length of the two complexes. After DSC/target DNA triple were incubated for 100 min at 37 °C with the introduction of λ exo, two new stripes (the same with the stripes in Lane 1 and Lane 2) were shown up. And DSC/target DNA triple stripe got weaker as expected, revealing that λ exo could hydrolyze non-phosphorylated PP in the presence of target DNA and aided the recycling of target DNA. Hence, the results obtained from 12% native PAGE could confirm the feasibility of the novel amplification method based on λ exo and non-phosphorylated dsDNA substrate. The LNTR only needs an incomplete complementary DSC and λ exo for target DNA recycling. What's more, the 2-nt-protuding ends were designed at the 5′ ends of PP to replace 5′-PO_4 sites, avoiding costly group modification.

3.4. Optimization of the experiment variables of the biosensing system

To obtain optimal biosensing performance, the crucial reaction conditions of the method were investigated systematically. The ratio concentration of pDNA to DNA/AgNCs ($c_{pDNA}/c_{DNA/AgNCs}$) on AgDNCs had a significant influence on the current response since the number of

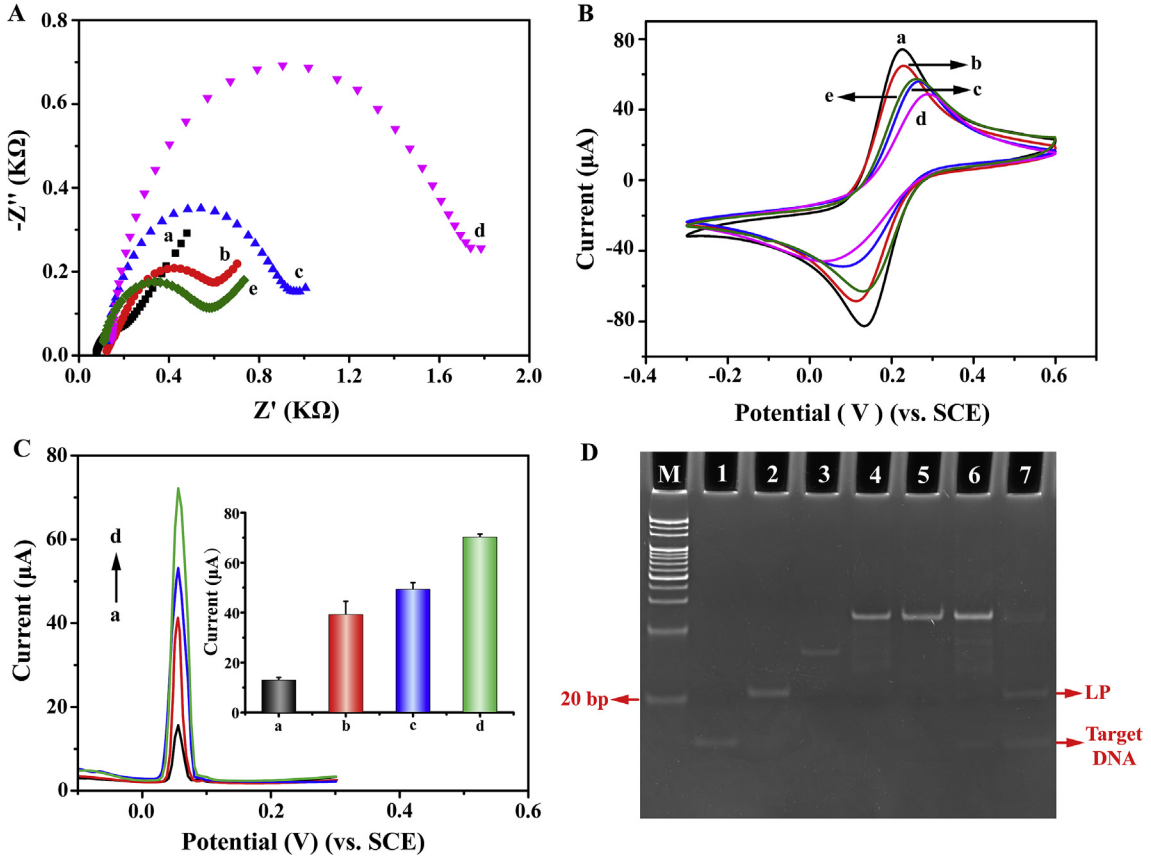

Fig. 3. (A) EIS and (B) CV at (a) bare gold electrode, (b) capture probes immobilized electrode, (c) after blocked with MCH, (d) after hybridized with LP of LNTR and (e) after hybridized with pDNA-AgDNCs@DNA/AgNCs conjugates in 0.1 M KCl containing 5 mM $Fe(CN)_6^{3-/4-}$ (pH 6.1). (C) DPV responses of the electrochemical DNA biosensor in the (a) absence and (d) presence of target DNA (1 nM), (b) the presence of target DNA (1 nM) without LNTR and (c) the presence of target DNA (1 nM) without DNA/AgNCs. Error bars: SD, n = 3. (D) 12% native PAGE analysis of LNTR: Lane M: 20 bp DNA ladder marker, Lane 1: target, Lane 2: LP, Lane 3: PP, Lane 4: DSC, Lane 5: DSC/λ exo, Lane 6: DSC/target DNA and Lane 7: DSC/target DNA/λ exo. (For interpretation of the references to color in this figure legend, the reader is referred to the Web version of this article.)

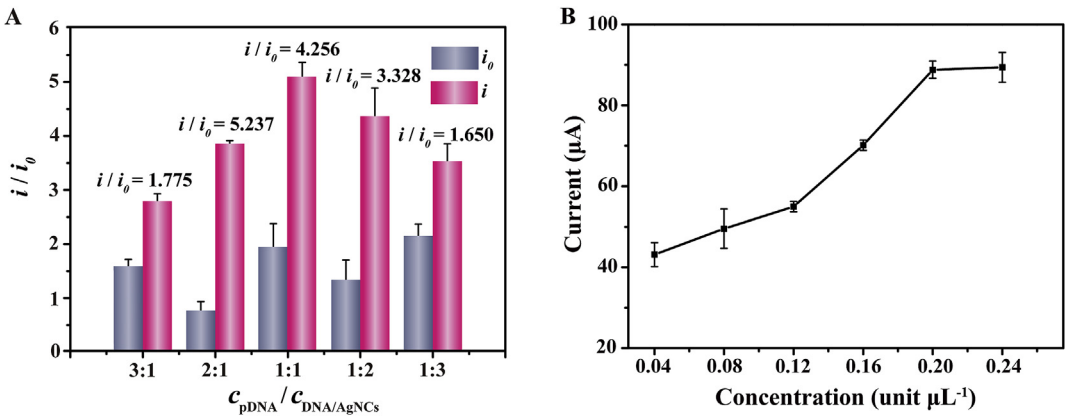

Fig. 4. The optimization of ratio concentration of (A) pDNA to DNA/AgNCs ($c_{pDNA}/c_{DNA/AgNCs}$) on AgDNCs (with the concentration of λ exo at 0.16 unit μL^{-1} and the LRA time for 80 min) and (B) the concentration of λ exo (with $c_{pDNA}/c_{DNA/AgNCs}$ at 2:1 and the LRA time for 80 min) for amplified detection of target (1 nM) by the proposed EBV-related biosensor. Error bars: SD, n = 3.

functional groups on the PAMAM dendrimers were fixed. Fig. 4A displayed the optimal signal-to-noise ratio corresponded to $c_{pDNA}/c_{DNA/AgNCs}$ was 2:1 (i/i_0, i and i_0 represent the DPV peak currents in the presence and absence of the target DNA, respectively). When $c_{pDNA}/c_{DNA/AgNCs}$ was from 3:1 to 1:1, the i increased with the addition of DNA/AgNCs. Such increase was possibly due to the special structure of DNA/AgNCs whose rod-shaped neutral cluster core (i.e. Ag^0) was peripherally surrounded by base-bound Ag^+ (Schultz et al., 2013). Thus, the enhanced electrochemical oxidation capacity was realized. Besides, as $c_{pDNA}/c_{DNA/AgNCs}$ decreased from 1:1 to 1:3, the i gradually decreased, probably because of the reduced capture of LNTR outputs with the reduced pDNA. The best signal-to-noise ratio (S/N = 5.237) was obtained while the DNA/AgNCs and pDNA reached a relative equilibrium on the AgDNCs surface. Therefore $c_{pDNA}/c_{DNA/AgNCs}$ = 2:1 was employed in all subsequent experiments. λ exo could cleave the hybrid of DSC/target DNA to release the target DNA for recycling. The various

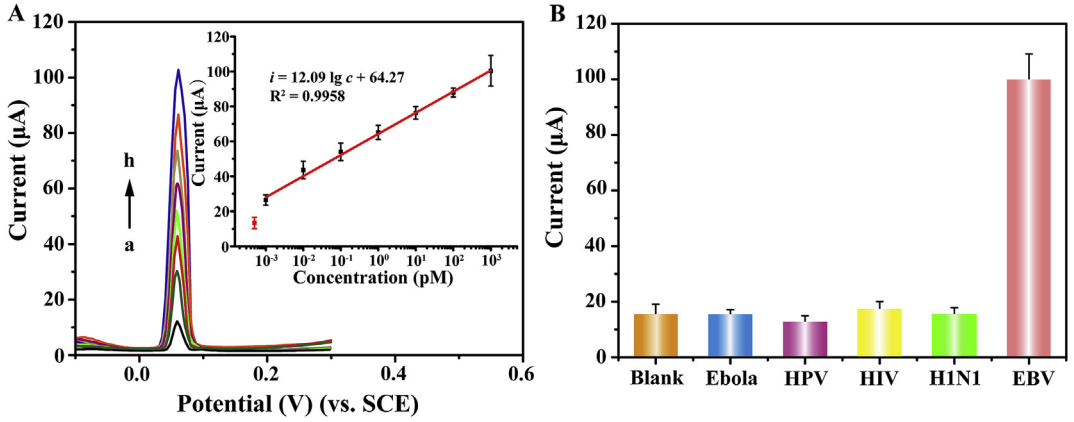

Fig. 5. (A) Typical DPV responses of the proposed EBV-related biosensor for different concentrations of the target: (a) 0 pM, (b) 0.001 pM, (c) 0.01 pM, (d) 0.1 pM, (e) 1.0 pM, (f) 10 pM, (g) 100 pM, (h) 1000 pM. The insert shows the calibration curve of the EBV-related biosensor. (B) Selectivity of the developed EBV-related biosensor: Blank (in the absence of the target DNA), Ebola-related DNA (1 nM), HPV-related DNA (1 nM), HIV-related DNA (1 nM), H1N1-related DNA (1 nM) and EBV-related DNA (1 nM). Error bars, SD, n = 3.

concentrations of λ exo were explored ranging from 0.04 unit μL^{-1} to 0.24 unit μL^{-1}. The DPV signal increased with the λ exo concentration and kept steady at 0.20 unit μL^{-1} (Fig. 4B). This was due to the fact the more enzymes, the faster the LNTR, and the output hybridized to the CP was nearly saturated. Consequently, 0.20 unit μL^{-1} was selected as the optimal λ exo concentration and used for subsequent experiments. A further study of incubation time of LNTR was performed (Fig. S2).

3.5. Analytical performance of EBV-related biosensor

The developed pDNA-AgDNCs@DNA/AgNCs conjugates and LNTR were committed to enhancing the sensitivity of the biosensing system. Under optimal experimental conditions, the DPV peak current increased linearly with the concentration of target DNA increasing from 1 fM to 1 nM (Fig. 5A). As depicted from the inset, the current response enlarged linearly with the logarithm of target DNA concentration between 1 fM to 1 nM. The determined linear regression equation was i (μA) = 12.09 × lg c (pM) + 64.27 (c represents the concentration of target DNA), and the regression coefficient (R^2) was 0.9958. A low detection of limit (LOD) of 0.38 fM was then calculated (S/N = 3). The sensitivity was lower than most of previously reported electrochemical DNA biosensor (Table S2), ascribing to the highly efficient electrical signal of dual-template encapsulated silver nanocomposites and the amplification effect of LNTR.

3.6. Specificity of the DNA biosensor and its application in real sample analysis

The selectivity of the proposed strategy was evaluated by using four different virus DNA sequences under the equal concentration (Ilkhani and Farhad, 2018; Sahoo et al., 2013; Shariati et al., 2019; Yan et al., 2018) (Table S1). As shown in Fig. 5B, the response signals of the DNA of the four control viruses DNA on the constructed label-free electrochemical platform were substantially identical to that of the blank test (bar Blank, background response without target DNA) and negligible change of electrochemical signal were observed. The strategy exhibited high fidelity in discriminating target DNA and other viral genes. This high specificity was attributed to the rigorous target DNA complement domain of PP and the specificity recognition effect of λ exo to DSC substrates.

An evaluation of the proposed biosensor's properties in biological conditions was evaluated by challenging the detection toward target DNA spiked in 1% human serum samples. The comparable results of different concentrations of target DNA at 10 fM, 1 pM, 100 pM in the complex matrix were shown in Table S3. The recoveries were 101–110% and CV (%) were below 5%, indicating the reliable and potential application of the proposed ultrasensitive electrochemical DNA biosensor in a relatively complex biological sample.

4. Conclusion

In summary, we have constructed a label-free and simple electrochemical biosensor for the ultrasensitive detection of EBV-related DNA *via* dual-template enhanced electroactive tags and λ exo-assisted target recycling. The fabricated electrochemical tags not only possess excellent redox performance by coupling AgNCs and DNA/AgNCs but also provide ideal nanocarrier with larger surface area. The ingenious designed DSC for λ exo allowed to recycle target DNA with high specificity and no modification. The developed biosensor exhibited ultrasensitivity, excellent specificity, good biocompatibility and acceptable matrix effect. This strategy has the potential for various target DNA analysis by changing recognition domain in PP. Thus, we anticipate that the developed electrochemical DNA biosensor could be a facile and alternative platform for the early diagnosis of EBV infection diseases and other biomedical research. Nevertheless, the subsequent fixing steps are still required for the products of LNTR, a further improvement can be made to simplify detection procedure in sandwich electrochemical biosensor.

Conflict of interest

The authors declare that they have no known competing financial interests or personal relationships that could have appeared to influence the work reported in this paper.

CRediT authorship contribution statement

Haiying Que: Conceptualization, Methodology, Software, Investigation, Data curation, Writing - original draft, Project administration. **Decai Zhang:** Software, Writing - review & editing, Investigation. **Bin Guo:** Methodology, Formal analysis, Software. **Tong Wang:** Conceptualization, Data curation. **Haiping Wu:** Resources, Software. **Daobin Han:** Resources, Validation. **Yurong Yan:** Supervision, Methodology, Data curation, Funding acquisition, Project administration, Data curation.

Declaration of competing interest

☒ The authors declare that they have no known competing financial interests or personal relationships that could have appeared to

influence the work reported in this paper.

Acknowledgements

This work was funded by the National Natural Science Foundation of China (81371904), the Natural Science Foundation Project of Chongqing (cstc2018jcyjAX0349) and the Top-notch Personnel Project of Chongqing Medical University (BJRC201822).

Appendix A. Supplementary data

Supplementary data to this article can be found online at https://doi.org/10.1016/j.bios.2019.111610.

References

Aoki, H., 2015. Chem. Asian J. 10, 2560–2573.
Balvedi, R.P., Castro, A.C., Madurro, J.M., Brito-Madurro, A.G., 2014. Int. J. Mol. Sci. 15, 9051–9066.
Bian, X., Guo, B., Zhao, M., Han, D., Cheng, W., Song, F., Ding, S., 2019. ACS Appl. Mater. Interfaces 11, 3715–3721.
Chen, L., Sha, L., Qiu, Y., Wang, G., Jiang, H., Zhang, X., 2015. Nanoscale 7, 3300–3308.
Chen, Z., Liu, Y., Xin, C., Zhao, J., Liu, S., 2018. Biosens. Bioelectron. 113, 1–8.
Dong, H., Jin, S., Ju, H., Hao, K., Xu, L.P., Lu, H., Zhang, X., 2012. Anal. Chem. 84, 8670–8674.
Han, D., Wei, C., 2018. Talanta 181, 24–31.
Hu, Y., Zhang, Q., Guo, Z., Wang, S., Du, C., Zhai, C., 2017. Biosens. Bioelectron. 98, 91–99.
Huang, J.F., Luo, H., Liang, C., Sun, I.W., Baker, G.A., Dai, S., 2005. J. Am. Chem. Soc. 127, 12784–12785.
Ilkhani, H., Farhad, S., 2018. Anal. Biochem. 557, 151–155.
Jie, G., Tan, L., Zhao, Y., Wang, X., 2017. Biosens. Bioelectron. 94, 243–249.
Jin, X., Zhou, L., Zhu, B., Jiang, X., Zhu, N., 2018. Biosens. Bioelectron. 107, 237–243.
Kangkamano, T., Numnuam, A., Limbut, W., Kanatharana, P., Vilaivan, T., Thavarungkul, P., 2018. Biosens. Bioelectron. 102, 217–225.
Kovall, R., Matthews, B.W., 1997. Science 277, 1824–1827.
Lee, C.Y., Park, K.S., Jung, Y.K., Park, H.G., 2017. Biosens. Bioelectron. 93, 293–297.
Li, X., Guo, J., Zhai, Q., Xia, J., Yi, G., 2016. Anal. Chim. Acta 934, 52–58.
Liu, S., Gong, H., Wang, Y., Wang, L., 2016. Biosens. Bioelectron. 77, 818–823.
Liu, Y., Huang, C.Z., 2012. Analyst 137, 3434–3436.
Lyu, D., Li, J., Wang, X., Guo, W., Wang, E., 2019. Anal. Chem. 91, 2050–2057.
Maduraiveeran, G., Sasidharan, M., Ganesan, V., 2018. Biosens. Bioelectron. 103, 113–129.
Miao, X., Cheng, Z., Ma, H., Li, Z., Xue, N., Wang, P., 2018. Anal. Chem. 90, 1098–1103.
Mu, W.Y., Yang, R., Robertson, A., Chen, Q.Y., 2018. Colloids Surfaces B Biointerfaces 162, 427–431.
New, S.Y., Lee, S.T., Su, X.D., 2016. Nanoscale 8, 17729–17746.
Peng, X., Zhu, J., Wen, W., Bao, T., Zhang, X., He, H., Wang, S., 2018. Biosens. Bioelectron. 118, 174–180.
Qiu, Z., Shu, J., Jin, G., Xu, M., Wei, Q., Chen, G., Tang, D., 2016. Biosens. Bioelectron. 77, 681–686.
Sahoo, P., Suresh, S., Dhara, S., Saini, G., Rangarajan, S., Tyagi, A.K., 2013. Biosens. Bioelectron. 44, 164–170.
Schultz, D., Gardner, K., Oemrawsingh, S.S., Markesevic, N., Olsson, K., Debord, M., Bouwmeester, D., Gwinn, E., 2013. Adv. Mater. 25, 2797–2803.
Shariati, M., Ghorbani, M., Sasanpour, P., Karimizefreh, A., 2019. Anal. Chim. Acta 1048, 31–41.
Shi, X.M., Fan, G.C., Tang, X., Shen, Q., Zhu, J.J., 2018. Biosens. Bioelectron. 109, 190–196.
Sorsak, E., Valh, J.V., Urek, S.K., Lobnik, A., 2015. Analyst 140, 976–989.
Stofik, M., Stryhal, Z., Maly, J., 2009. Biosens. Bioelectron. 24, 1918–1923.
Tang, Y., Chai, Y., Liu, X., Li, L., Yang, L., Liu, P., Zhou, Y., Ju, H., Cheng, Y., 2018. Biosens. Bioelectron. 117, 224–231.
Wu, T., Yang, Y., Chen, W., Wang, J., Yang, Z., Wang, S., Xiao, X., Li, M., Zhao, M., 2018. Nucleic Acids Res. 46, 3119–3129.
Yan, X., Tang, M., Yang, J., Diao, W., Ma, H., Cheng, W., Que, H., Wang, T., Yan, Y., 2018. RSC Adv. 8, 31710–31716.
Yang, C., Shi, K., Dou, B., Xiang, Y., Chai, Y., Yuan, R., 2015. ACS Appl. Mater. Interfaces 7, 1188–1193.
Zeng, J., Zheng, Y., Rycenga, M., Tao, J., Li, Z.Y., Zhang, Q., Zhu, Y., Xia, Y., 2010. J. Am. Chem. Soc. 132, 8552–8553.
Zhang, K., Huang, W., Li, H., Xie, M., Wang, J., 2019. Biosens. Bioelectron. 132, 310–318.
Zhou, L.Y., Zhang, X.Y., Wang, G.L., Jiao, X.X., Luo, H.Q., Li, N.B., 2012a. Analyst 137, 5071–5075.
Zhou, T., Huang, Y., Li, W., Cai, Z., Luo, F., Yang, C.J., Chen, X., 2012b. Nanoscale 4, 5312–5315.
Zhou, Z., Wang, Y., Yan, Y., Zhang, Q., Cheng, Y., 2016. ACS Nano 10, 4863–4872.